



Hybrid P3HT: PCBM/GaN nanowire/Si cascade heterojunction for photovoltaic application

Giorgi Tchutchulashvili · Krzysztof P. Korona · Wojciech Mech · Sergij Chusnutdinow · Marta Sobanska · Kamil Klosek · Zbigniew R. Zytkeiwicz · Wojciech Sadowski

Received: 31 October 2019 / Accepted: 27 February 2020 / Published online: 29 March 2020
© The Author(s) 2020

Abstract Poly (3-hexylthiophene) (P3HT) and phenyl-C61-butyric acid methyl ester (PCBM) are commonly used for the fabrication of organic photovoltaics (OPV). Efficiency limitations of OPVs could be circumvented by incorporation of inorganic nanostructures into organic blends. Again, integration of organic solar cells with well-developed silicon photovoltaic technology is ultimately desirable. In the present work, GaN nanowires with diameters of 25–50 nm and two lengths (200 and 500 nm) have been grown using molecular beam epitaxy technique. Solar-grade monocrystalline silicon wafers were used as substrates for nanowire synthesis. GaN nanostructures were incorporated into P3HT:PCBM photoactive layer in order to facilitate charge transfer between P3HT:PCBM and Si. Samples with and without nanowires were compared. Addition of nanowires led to the improvement in photovoltaic performance. Open circuit voltage has risen by 72% and short circuit current density by 200%. Series resistance has decreased

50 times, and power conversion efficiency has risen 20.7 times. Additional maxima are found in photocurrent spectrum corresponding to carriers being generated near GaN absorption edge. Moreover, external quantum efficiency peaks near GaN absorption edge, indicating the formation of current transfer channel via P3HT/GaN/Si cascade heterojunction. Mechanism explaining source of abovementioned improvement is proposed.

Keywords GaN nanowires · P3HT · PCBM · Solar cells · Molecular beam epitaxy · Energy conversion

Introduction

Application of inorganic materials as photo electrodes in organic solar cells has attracted significant interest since they potentially improve the performance of such solar cells (Zhang and Liu 2019). Most of the modern organic solar cells are based on bulk heterojunction (BHJ) where donor and acceptor materials are intermixed on nanoscale (Yu et al. 1995). Charge transport inside BHJ remains one of the main challenges for organic photovoltaics, causing current density bottleneck and degraded performance (Holliday et al. 2017). Organic solar cell improvement using carbon nanotubes (Feng et al. 2013), inorganic nanostructures (Arici et al. 2003; McDonald et al. 2005; Choudhury et al. 2005; Hau et al. 2008; Kwak et al. 2009; Oh et al. 2013), metal nanorods (Kim et al. 2011), and inorganic nanowires (Wang et al. 2011; Davenas et al. 2012; Das et al. 2011) has been reported in literature.

G. Tchutchulashvili (✉) · W. Sadowski
Faculty of Applied Physics and Mathematics, Gdansk University of Technology, Gabriela Narutowicza 11/12, 80-233 Gdansk, Poland
e-mail: giorgi.tchutchulashvili@pg.edu.pl

K. P. Korona · W. Mech
Faculty of Physics, University of Warsaw, Pasteura 5, 02-093 Warsaw, Poland

G. Tchutchulashvili · S. Chusnutdinow · M. Sobanska · K. Klosek · Z. R. Zytkeiwicz
Institute of Physics, Polish Academy of Sciences, al. Lotników 32/46, 02-668 Warsaw, Poland

Nanowires used as an acceptor material in bulk heterojunction provide high junction area as well as uninterrupted conductive channels that ensure the efficient collection of carriers generated in the device (Kannan et al. 2003; Hoppe and Sariciftci 2006). Additionally, structures with mutually aligned nanowires synthesized directly on silicon could be used as an intermediate layer in multijunction solar cells, combining organic excitonic solar cells with conventional silicon photovoltaics, if the method for efficient charge transfer between organic heterojunction and silicon could be identified.

Despite large amount of works discussing ways of improving thiophene-based solar cells, there are little reports on P3HT/GaN system. This field was established by works exploring electrical behavior of P3HT/GaN interfaces (Park et al. 2009; Kumar et al. 2013), and others report organic structures with GaN nanoparticles synthesized by sol-gel method (Feng et al. 2013) and hybrid vapor phase epitaxy grown GaN quantum dots (Kim et al. 2013). A more recent paper by Noh et al. (2017) discusses photovoltaic performance of P3HT layers deposited on planar GaN. Still to date, reports discussing thiophene-based photovoltaics with GaN nanowire acceptors are scarce, despite the fact that techniques of GaN nanowire growth are well-developed. Authors are convinced that the presented results will deepen our understanding of physical processes occurring in P3HT/GaN photovoltaic system.

In this paper, we report on the fabrication and characterization of P3HT:PCBM/GaN nanowires/Si (BHJ/GaN NWs/Si) hybrid organic-inorganic films consisting from a structure of vertical monocrystalline GaN nanowires (GaN NWs) grown on silicon substrate and embedded in P3HT:PCBM blend (Fig. 1). Theoretical alignment of energy levels (Park et al. 2009; Pyrgotakis 2014) seen in Fig. 8b shows that P3HT:PCBM/GaN NWs form a cascade type II heterojunction, which permits efficient exciton dissociation and transport through BHJ (Fig. 1b). Generated current is then transferred to the silicon substrate through the GaN/Si_xN_y/Si interface.

Experimental

Samples studied in this work were obtained by spinning of P3HT:PCBM films onto the following inorganic acceptor structures: n and p-type silicon (no nanowires, organic film thickness of 200 nm), 500 nm GaN

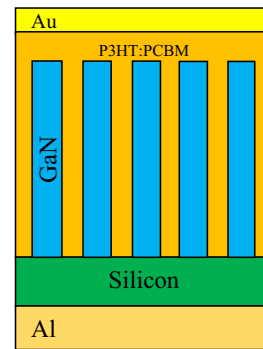


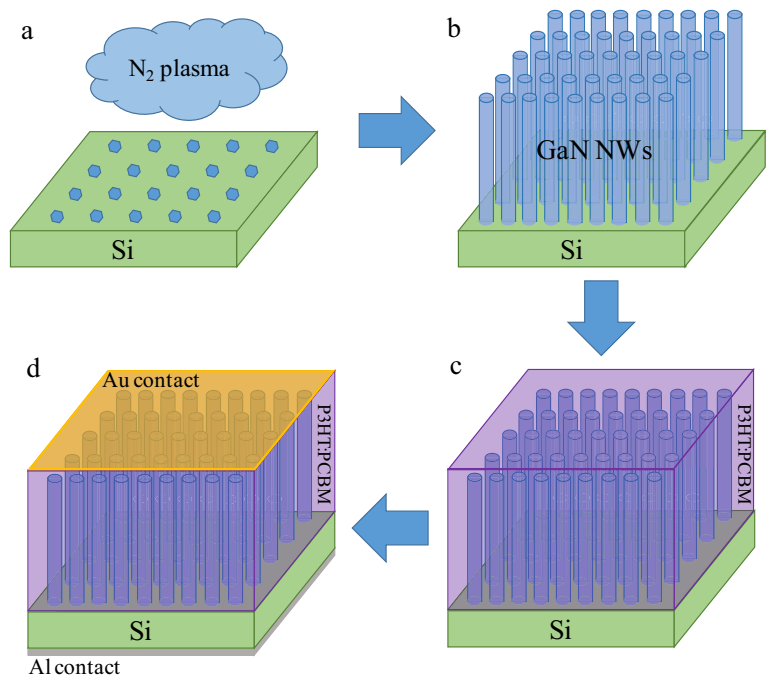
Fig. 1 Schematic drawing of a hybrid structure cross-section

nanowires grown on n- and p-type silicon, and 200 nm GaN nanowires on n-type Si. In all cases, silicon substrate resistance was $\sim 1 \Omega \text{ cm}$ and thickness was $380 \mu\text{m}$.

Fabrication procedure of the structures is shown in Fig. 2. First, after silicon oxide desorption inside the growth chamber, $\sim 2 \text{ nm}$ thick silicon nitride nucleation layer was formed on the Si (111) surface by its exposure to nitrogen plasma for 15 min at $750 \text{ }^\circ\text{C}$ (Wierzbicka et al. 2013). The silicon nitride layer is sufficiently thin to allow the flow of electric current through the GaN/Si interface. This stage was also completed for samples with no nanowires to correctly model charge transfer conditions through the P3HT:PCBM/Si interface of samples after GaN NW growth. After nucleation, self-assembled NW growth was conducted by plasma-assisted molecular beam epitaxy (PAMBE) under N-rich conditions at $785 \text{ }^\circ\text{C}$ (Fig. 2b). On this stage area, the distribution of nanowires and thus the period of NW structure is determined by controlling substrate temperature and Ga flux. GaN nanowires were n-type doped with Si. Charge carrier concentration in the nanowires was estimated to be $5 \times 10^{18} \text{ cm}^{-3}$ basing on the calibration of the Si flux on reference planar GaN samples. Nanowire length is controlled by growth time. Details of PAMBE growth procedure can be found elsewhere (Borysiuk et al. 2014; Sobanska et al. 2016; Korona et al. 2014).

Regioregular P3HT with an average molecular weight of $54,000\text{--}75,000 \text{ g/mol}$ was mixed with PCBM in chloroform solution in concentrations 15 mg/ml for P3HT and 10 mg/ml for PCBM. Both materials of electronic purity were purchased from Sigma-Aldrich. Blend was mixed for 24 h at $40 \text{ }^\circ\text{C}$ and then cooled to room temperature and filtered through the $0.45 \mu\text{m}$ syringe filter.

Fig. 2 Schematic diagrams of BHJ/GaN NWs/Si fabrication process: **a** creation of silicon nitride layer for nanowire nucleation; **b** nanowire growth; **c** spin-coating with organic blend and annealing; **d** contact deposition



Inorganic acceptors were spin-coated with organic blend at 2000 RPM for 30 s (Fig. 2c). This produced thin films with a thickness of 200 nm for given precursor viscosity. Devices were annealed on a hot plate at 150 °C for 15 min. All steps involving organic blend preparation were conducted in dry argon atmosphere. Finally, electrical contacts were deposited using RF sputtering technique on Quorum Technologies Q150T equipment. The 2×2 mm rectangular golden contacts with 20% measured transparency were deposited on polymer surface (Fig. 2d). Thick Al film was used as bottom contact to Si. In order to gather sufficient statistics, at least four samples were prepared for every variant of studied structure, each of them housing minimum four individual solar cells. Measurement results shown in this contribution were averaged from obtained massive data.

Photocurrent spectroscopy (PCS) measurements were performed in the spectral range from 300 to 1400 nm (1.24–4.2 eV) using the light of the tungsten lamp passing through the monochromator. The current was measured in a short circuit mode (I_{sc}) with a Keithley picoammeter, so the I_{sc} spectra, i.e., the short-circuit photocurrent vs. light wavelength dependence, were registered. Since the spectral power of light, $P(h\nu)$

was measured; it was possible to determine the external quantum efficiency,

$$EQE(h\nu) = \frac{h\nu I_{sc}(h\nu)}{eP(h\nu)} \quad (1)$$

where $h\nu$ is incident photon energy, I_{sc} is the photocurrent measured in short circuit mode, and e is the elementary charge. The spectra were obtained using a tungsten lamp that has maximum power in infrared at about 1 eV. Since the light was filtered by monochromator, the light intensity was low; it was of the order of 1% of AM1.5. Therefore, the external quantum efficiency (EQE) spectra, especially for samples with high leakage current, can be underrated. In such case, photocurrent integrated over the spectrum can differ compared to photocurrent generated by simulated sun radiation.

The device J-V characteristics under simulated solar spectrum were measured using PEQUEST solar simulator equipped with RERA Solution station with Tracer 2 software package, Keithley 2601A measure unit, and LOT Oriel 300 watt Xe light source with AM1.5 filter, calibrated at 1000 W cm^{-2} irradiance using standard silicon reference cell.

Photovoltaic performance parameters of hybrid films were obtained from J-V dependences. Series and shunt resistances were extracted by manual fitting with Shockley diode equation:

$$J = J_{ph} - J_0 \left[\exp \left\{ \frac{q(V + JR_s)}{nk_B T} \right\} - 1 \right] - \frac{V + JR_s}{R_{sh}} \quad (2)$$

where J_{ph} is the photocurrent density, J_0 is the diode saturation current, R_s is the series resistance, R_{sh} is the shunt resistance, q is the electron charge, n is the ideality factor, k_B is the Boltzmann constant, and T is the absolute temperature.

The ideality factor was extracted from semi-logarithmic J-V plots. First, curve slope was determined in the 0.4–0.5 V voltage range using the equation:

$$m = \frac{d \log J}{dV} \quad (3)$$

from where the ideality factor was calculated using the relationship (Schroder 2009):

$$n = \frac{q}{2.3mk_B T} \quad (4)$$

Scanning electron microscopy (SEM) characterization of nanowires was performed using Hitachi SU-70 field emission scanning electron microscope. The EDX system is equipped with Thermo Scientific UltraDry EDX Detector and Noran System Seven software. The signal from secondary electron detector was used to obtain top view and cross-sectional images of the as-grown nanowires. In order to determine their elemental composition, individual nanowires were detached from the Si substrate and dispersed on a holey carbon film on a 300 mesh copper grid. To efficiently excite the X-ray line with an electron beam, critical ionization energy of the element of interest must be exceeded by a factor of 1.5–3. Hence recording of Ga line at 9.241 keV required accelerating voltage of at least 15 kV. Atomic concentrations of nitrogen, gallium, and dopant silicon were calculated from the collected X-ray spectrum. Measurements were performed in field-free mode.

Results and discussion

Figure 3 shows scanning electron microscope images of the GaN NWs morphology. As seen, PAMBE growth results in vertically aligned nanowires. Figure 3a and b show cross-sectional images of NW with lengths of 500 nm and 200 nm, respectively. Figure 3c illustrates

typical distribution of nanowires on the substrate surface. Nanowire diameters fall in the 25–50 nm range. The period of nano-patterned interface is defined as an average distance between nanowires and it equals to 60–65 nm as measured by the ImageJ software from plane view SEM images. Figure 3d shows the cross-section of a finished 500 nm thick structure. Organic blend covers a whole stack of nanowires, including nanowire side walls and reaches the silicon surface. Outstretched lumps of polymer closer to the top of the layer appear due to bad cleavage of the polymer foil. The top of structure is coated with golden electrode which forms continuous film.

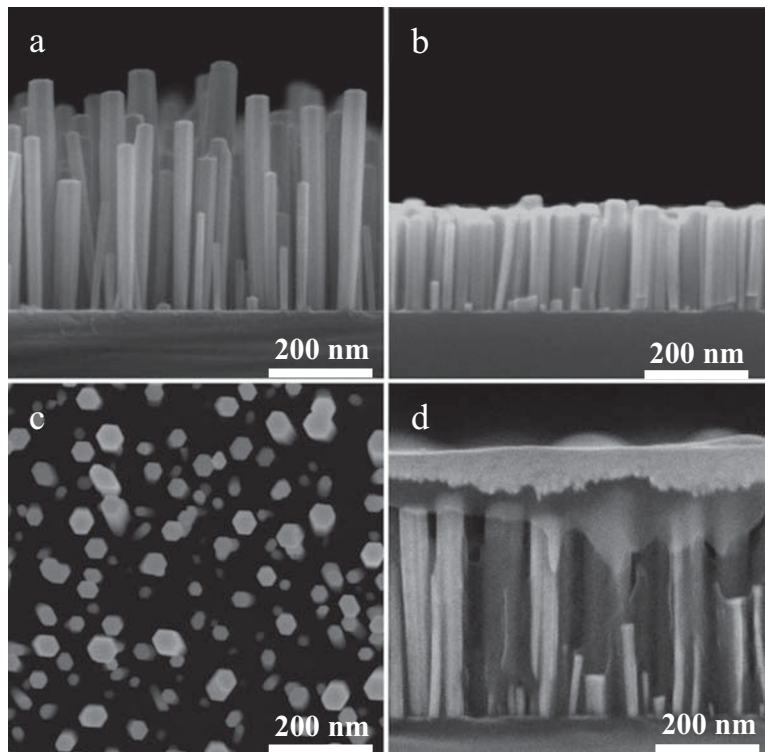
Furthermore, nanowires were dispersed onto copper mesh and studied by EDX spectroscopy (Fig. 4a). Clearly distinguishable gallium (1.098 KeV and 9.241 KeV), nitrogen (0.392 KeV), and silicon (1.739 KeV) pikes could be seen in X-ray spectrum on Fig. 4b. Quantitative analysis gives proportion of atomic concentrations Ga:N:Si = 65.5:34:0.8%. However, spectrum collected at 15 keV could miss nitrogen, because of low atomic number of that element.

Figure 5a presents current density-voltage characteristics of films containing no GaN NWs. Parameters extracted from J-V curves are collected in Table 1. It is instantly obvious that the net performance of the structure depends on the conductivity type of silicon substrate. The inferior performance achieved on p-type silicon substrates can be explained by assumption that junction between P3HT and silicon is of Schottky type. Consequently, direction of the current through P3HT/Si interface depends on silicon conductivity type. Specifically, in the case of films fabricated on n-type silicon, the direction of photocurrent contributed by P3HT/Si interface is the same as total photocurrent generated in the structure. Situation is opposite for films deposited on p-Si. Moreover, photocurrent spectrum for BHJ/p-Si structure (Fig. 5b) shows negative current (dotted line) at incident photon energy range corresponding to the situation when only BHJ/Si interface is activated as organic film is transparent for photons below 1.9 eV. To explain such behavior one can present structures total photocurrent by sum of its components:

$$J_{total} = J_{BHJ} + J_{BHJ/Si} \quad (5)$$

where J_{BHJ} represents current originating from photoactivation and excitons separation on P3HT:PCBM bukl heterojunction, and $J_{BHJ/Si}$ is the current generated when organic blends interface with silicon substrate is

Fig. 3 SEM images of GaN NWs: **a** and **b** cross-sectional view of 500 and 200 nm long nanowires, **c** plane view showing typical nanowire density, **d** cross-sectional image of finished structure



activated. Notably, J_{BHJ} approaches zero for energies below 1.9 eV because organic film is transparent for low energy photons. $J_{\text{BHJ/Si}} > 0$ for n-Si resulting in photocurrent maximum seen near silicon absorption edge (Fig. 5b). $J_{\text{BHJ/Si}} < 0$ for p-Si giving negative net current for lower energies and positive but lower current for higher energies where J_{BHJ} component becomes relevant.

Next, silicon substrates were replaced by silicon with grown GaN nanowires. J-V and PCS characterization results are shown on Fig. 6. BHJ/200 nm, GaN NWs/n-Si, and BHJ/n-Si films have the same photoactive layer thickness and thus can be compared directly. The BHJ/200 nm GaN NWs/n-Si structure demonstrated $V_{\text{oc}} = 0.5$ V, $J_{\text{sc}} = 1.48 \text{ mA}\cdot\text{cm}^{-2}$, and FF = 39%. Addition of

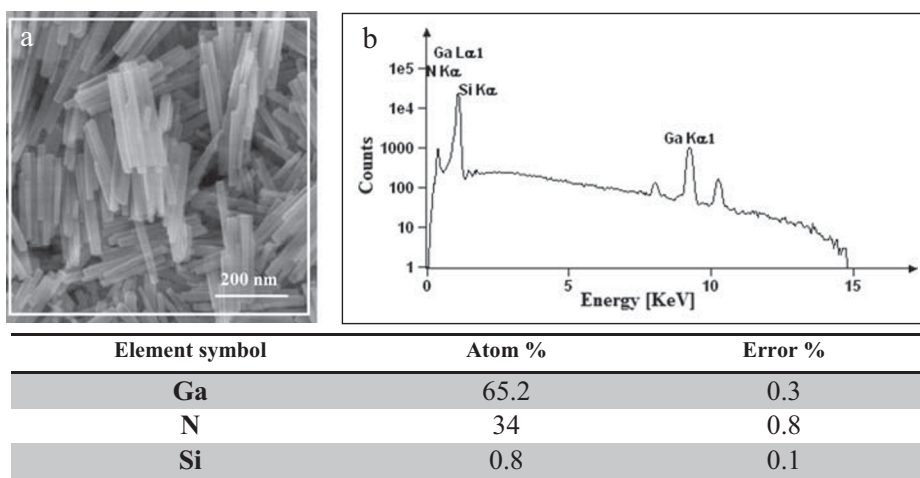


Fig. 4 EDX characterization results of GaN nanowires at accelerating voltage of 15 kV; **a** SEM image of dispersed nanowires acquired using secondary electron detector. White rectangle marks

the area from which EDX signal was collected. **b** X-ray spectrum of GaN nanowires with distinguishable Ga, N, and Si pikes. Quantitative data is shown in the table

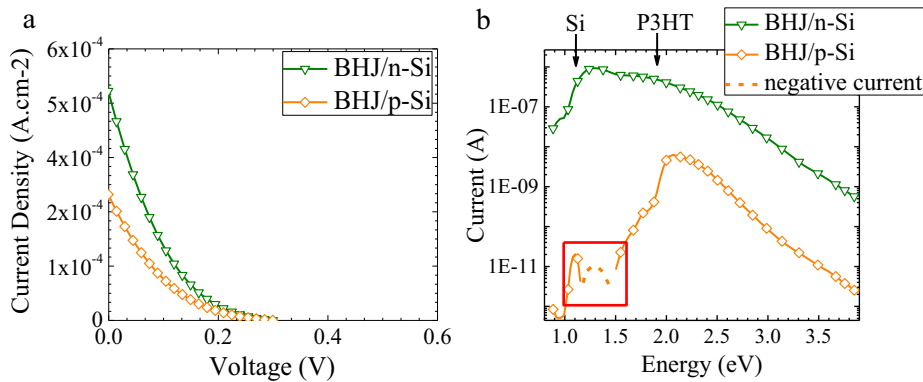


Fig. 5 **a** J-V plot for the illuminated pure BHJ layers deposited directly on n- and p-Si substrates. **b** Photocurrent spectra of the same structures. Marked red with red square is a negative current generated by BHJ/p-Si structure in 1.1–1.4 V range (color online)

nanowires to the BHJ/Si interface led to the improvement of all photovoltaic performance parameters (Table 1). Open circuit voltage has risen by 72%, short circuit current density by 200%, and FF by 3.9 times. Significant impact has addition of GaN nanowires on series and shunt resistances of the structure. Specifically, 50 times decrease in R_s together with 5.8 times rise in R_{sh} was observed. PCE of BHJ/200 nm GaN NW/n-Si is 0.29% what constitutes 20.7 times increase vs. similar structure without GaN NWs. For comparison, results reported by Kim et al. (2013) for P3HT/GaN quantum dots hybrid heterojunction show: $V_{oc} = 0.16$ V, $J_{sc} = 3.6$ mA.cm⁻², and FF = 25%, respectively.

Improvement in structures performance is probably caused by better charge separation and collection conditions in the presence of nanowires. Especially important role nanowires play in transferring photocarriers from BHJ to silicon substrate. Larger FF value shows that nanowires enhance electrical conductivity of organic bulk heterojunction in vertical direction. Still, R_s of 200 nm GaN structure equals hundreds of ohms which is a large value compared to single ohm state-of-the-art solar cells. High R_s is probably caused by high resistance of interface of active layers with silicon. Even after R_s is decreased due to application of GaN nanowires, resistance of whole

380 μ m thick silicon substrate itself contributes to series resistance of hybrid junction resulting in resistance higher than that of a typical thin-film solar cell.

Comparison of J-V characteristics of BHJ/200 nm GaN NWs/n-Si and BHJ/500 nm GaN NWs/n-Si (Fig. 6a) gives the information about dependence of film properties on BHJ layer thickness. Although, 500 nm thick film demonstrates better J_{sc} , its open circuit voltage, fill factor, and R_s are inferior, due to losses on higher series resistance of 500 nm film outmatching gain from increased light absorption in thicker polymer layer. As in the case of BHJ/p-Si film, performance of BHJ/500 nm GaN NW/p-Si is inferior due to similar reasons. Equation 5 is similar for the structures with nanowires with additional photocurrent component $J_{BHJ/GaN}$, generated by illuminated BHJ/GaN interface.

$$J_{total} = J_{BHJ} + J_{BHJ/Si} + J_{BHJ/GaN} \quad (6)$$

In voltage range 1–1.9 eV structure behaves similarly to pure blends on silicon. After P3HT absorption edge the photocurrent becomes equal, without difference associated with silicon conduction type. We assume that photoelectrons from excited P3HT are mostly transferred to GaN. There is a tunnel junction on n-Si/

Table 1 Performance parameters of hybrid films

Hybrid structure	$V_{oc}[V]$	$J_{sc}[mA.cm^{-2}]$	FF[%]	$R_s[\Omega]$	$R_{sh}[k\Omega]$	n	PCE [%]
BHJ/n-Si (200 nm)	0.29	0.49	10	1.7×10^4	1429	2.61	0.014
BHJ/p-Si (200 nm)	0.3	0.28	11	2.2×10^4	625	2.98	0.01
BHJ/200 nm GaN NWs /n-Si	0.5	1.48	39	345	8265	1.26	0.29
BHJ/500 nm GaN NWs/n-Si	0.46	2.37	24	769	350	1.99	0.26
BHJ/500 nm GaN NWs/p-Si	0.31	0.61	29	1515	1639	1.58	0.06



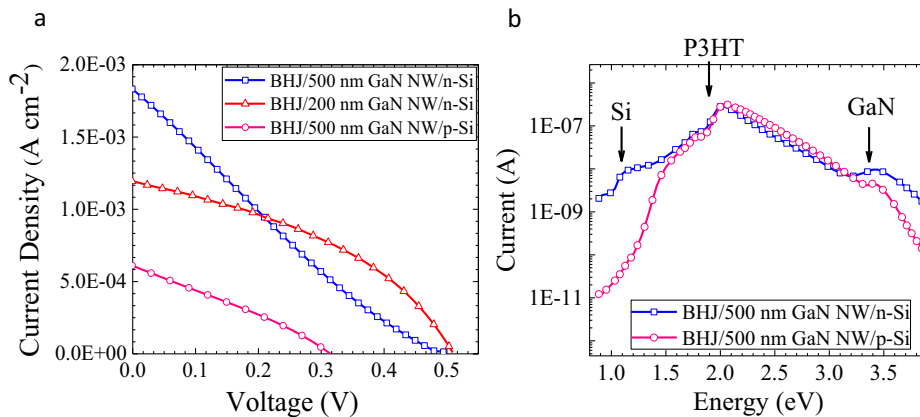


Fig. 6 **a** Illuminated J-V plots for hybrid structures with GaN NWs. **b** Photocurrent spectra of BHI/500 nm GaN NW/n-Si and BHI/500 nm GaN NW/p-Si (color online)

Si3N4/GaN interface (band diagram in Fig. 8b) which does not have rectifying behavior. Lastly, a distinct photocurrent pike is seen at GaN absorption edge.

External quantum efficiency spectra calculated from the PCS data are plotted in Fig. 7. BHI/n-Si curve shows EQE maxima at Si and P3HT absorption edges. BHI/p-Si plot confirms low efficiency of BHI/p-Si interface in photoexciton separation. Particularly interesting are the efficiencies of BHI/GaN NWs/Si films which show increase towards higher energies of incident light reaching maximum value of EQE = 0.32 at GaN absorption edge. The presence of this peak proves high efficiency of electron extraction from organic blend by GaN NWs. EQE of the component of photocurrent seen in the vicinity of silicon absorption edge in Fig. 5b is weak, so we conclude that the main contributors to photocurrent in the BHI/GaN

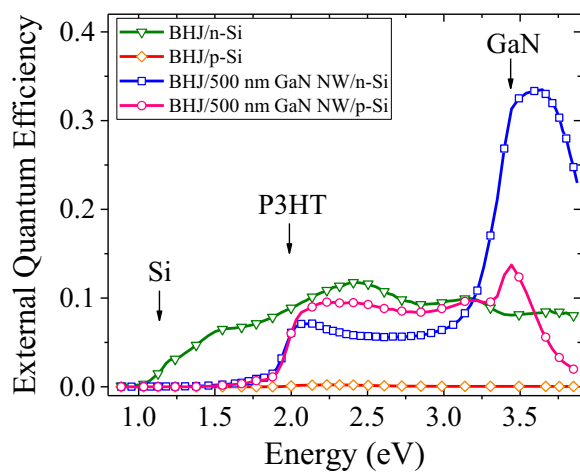


Fig. 7 Comparison of EQE spectra for hybrid structures with and without GaN nanowires deposited on n- and p-Si substrates (color online)

NWs/Si architecture are P3HT:PCBM blend and GaN nanowires. This finding demonstrates the high potential of crystalline GaN nanowires to enhance the efficiency of charge carrier separation and collection, essential for photovoltaic application. Further studies are necessary to determine the optimal hybrid film thickness and nanowire period for BHI/GaN NWs/n-Si structure.

Basing on experimental observations presented above, we propose a mechanism explaining charge transfer in the BHI/GaN NWs/Si cascade heterojunction. The mechanism is schematically illustrated in Fig. 8a and corresponding theoretical band diagram in Fig. 8b. Strongly bound excitons are being created during incident photon absorption by P3HT molecule. The excitons generated inside the cylindrical volume around the nanowire defined by exciton diffusion length have a higher chance of being dissociated on the P3HT/GaN NWs interface and use favorable band alignment P3HT:PCBM:GaN. Resulting photocurrent component is marked as “a”. Excitons originating from outside this volume are dissociated by the P3HT:PCBM blend and then PCBM passes electron to GaN (component a’). Which of these two processes, a or a’, is more efficient in charge carrier generation would depend on nanowire structure period. Whenever the charge transfer is a result of a or a’ process, after electron reaches GaN it is conducted through the nanowire b and collected by the Si substrate. Photocurrent component c is a result of electron generation in P3HT, its transfer first to PCBM and then to Si. Components a, a’, b, and c together give current J_{BHI} in eq. 6. Electrons generated inside volume adjacent to region of the P3HT/Si Schottky junction are pushed towards cathode, while holes are injected from Si into organic blend giving current c' ($J_{BHI/Si}$ in eq. 6). Electrons injected into organic

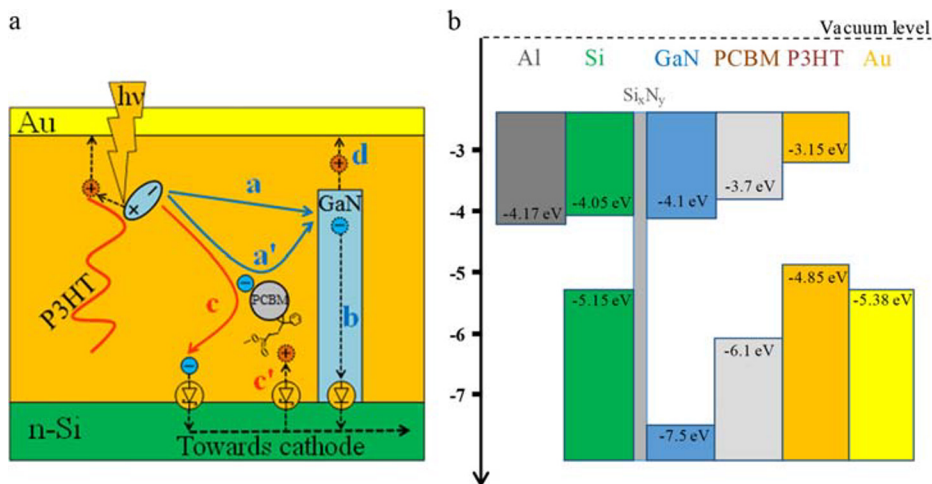


Fig. 8 **a** Mechanism explaining electric current generation processes in BJJ/GaN NWs/Si cascade junction. Following photocurrent components are contributed by respective interfaces: **a** P3HT/GaN NW interface and **a'** by P3HT:PCBM blend. **b** electron

transport through GaN NW. **c** photoexcitation of P3HT:PCBM interface and electron transfer to the silicon; **c'** hole injection from silicon to organic blend. **d** hole injection from GaN. **b** Theoretical energy level diagram

blend from GaN result in current **d** ($J_{\text{BJJ/GaN}}$ in eq. 6). It is worth noticing that this mechanism also explains behavior of BJJ/Si structures without nanowires. In this case, currents **a**, **a'**, **b**, and **d** are equal to zero.

The mechanism depicted in Fig. 8 is very useful for understanding PCS data Fig. 6b and 7b. Difference in photocurrent between BJJ/n-Si and BJJ/p-Si structures can be explained by assuming that for BJJ/n-Si film currents **c** and **c'** have the same sign, while for BJJ/p-Si, these currents signs are opposite. Difference in photocurrent near Si absorption edge for the BJJ/500 nm GaN NWs/n-Si and the BJJ/500 nm GaN NWs/p-Si shown in Fig. 6b is also easily explained by switching direction of the P3HT/Si junction when Si substrate doping type is changed. It is evident from this mechanism that **a** and **a'** currents are almost unaffected by Si substrate conductivity type. This claim is supported by equal photocurrent values exhibited by both structures near P3HT absorption edge in Fig. 6b. These findings prove that P3HT:PCBM/GaN NW system has high potential for construction of multijunction solar cells with silicon-based cell as a bottom part.

Conclusions

In conclusion, we have examined photovoltaic structures with a P3HT:PCBM/GaN NWs/Si hybrid heterojunction. Structures were created by spin-coating of P3HT:PCBM organic blend onto GaN nanowire structures synthesized on solar-grade silicon by molecular beam epitaxy. We have

found that the incorporation of GaN nanowires into organic blend/silicon interface greatly enhances photovoltaic performance of a structure by facilitating efficient charge transfer between organic film and the substrate. Open circuit voltage was enhanced by 72%, short circuit current density by 200%, and FF by 3.9 times. PCE have increased 20.7 times compared to similar structure without GaN NWs. GaN nanowires also significantly reduced R_s of the hybrid film. EQE spectrum of cascade heterojunction shows increase towards wavelengths of incident light corresponding to GaN absorption edge, with maximum value of $EQE = 0.32$. Qualitative mechanism explaining charge transfer in hybrid structure is proposed. Authors hope these results are interesting in terms of designing hybrid multi-layer structures with nanostructured heterojunction.

Acknowledgments Authors want to thank A. Pieniążek and A. Reszka for EDX and SEM measurements.

Funding information This work was jointly supported from Polish National Science Centre grants No. 2016/21/B/ST5/03378, 2016/21/N/ST3/03381 and 2016/23/B/ST7/03745.

Compliance with ethical standards

Conflict of interest The authors declare that they have no conflict of interest.

Open Access This article is licensed under a Creative Commons Attribution 4.0 International License, which permits use, sharing, adaptation, distribution and reproduction in any medium or format, as long as you give appropriate credit to the original author(s) and

the source, provide a link to the Creative Commons licence, and indicate if changes were made. The images or other third party material in this article are included in the article's Creative Commons licence, unless indicated otherwise in a credit line to the material. If material is not included in the article's Creative Commons licence and your intended use is not permitted by statutory regulation or exceeds the permitted use, you will need to obtain permission directly from the copyright holder. To view a copy of this licence, visit <http://creativecommons.org/licenses/by/4.0/>.

References

- Arici E, Sariciftci NS, Meissner D (2003) Hybrid solar cells based on nanoparticles of CuInS_2 in organic matrices. *Adv Funct Mater* 13:2. <https://doi.org/10.1002/adfm.200390024>
- Borysiuk J, Zytewicz ZR, Sobanska M, Wierzbicka A, Klosek K, Korona KP, Perkowska PS, Reszka A (2014) Growth by molecular beam epitaxy and properties of inclined GaN nanowires on Si(001) substrate. *Nanotechnology* 25: 135610. <https://doi.org/10.1088/0957-4484/25/13/135610>
- Choudhury KR, Sahoo Y, Ohulchanskyy TY, Prasad PN (2005) Efficient photoconductive devices at infrared wavelengths using quantum dot-polymer nanocomposites. *Appl Phys Lett* 87:073110. <https://doi.org/10.1063/1.2011768>
- Das NC, Biswas S, Soko PE (2011) The photovoltaic performance of ZnO nanorods in bulk heterojunction solar cells. *J Renew Sustain Energy* 3:033105–033113. <https://doi.org/10.1063/1.3599838>
- Davenas J, Dkhil SB, Cornu D, Rybak A (2012) Silicon nanowire/P3HT hybrid solar cells: effect of the electron localization at wire nanodiameters. *Energy Procedia* 31:136–143. <https://doi.org/10.1016/j.egypro.2012.11.175>
- Feng Q, Shi P, Li Y-K, Du K, Wang Q, Feng Q, Hao Y (2013) Hybrid solar cell based on polythiophene and GaN nanoparticles composite. *Chin Phys B* 23(2). <https://doi.org/10.1088/1674-1056/23/2/028802>
- Hau SK, Yip HI, Acton O, Baek NS, Ma H, Jen A (2008) Interfacial modification to improve inverted polymer solar cells. *J Mater Chem* 18:5113–5119. <https://doi.org/10.1039/B808004F>
- Holliday S, Li Y, Luscombe CK (2017) Recent advances in high performance donor-acceptor polymers for organic photovoltaics. *Prog Polym Sci* 70:34–51. <https://doi.org/10.1016/j.progpolymsci.2017.03.003>
- Hoppe H, Sariciftci NS (2006) Morphology of polymer/fullerene bulk heterojunction solar cells. *J Mater Chem* 16:45–61. <https://doi.org/10.1039/B510618B>
- Kannan B, Castellino K, Majumdar A (2003) Design of nanostructured heterojunction polymer photovoltaic devices. *Nano Lett* 3(12):1729–1733. <https://doi.org/10.1021/nl034810v>
- Kim C-H, Cha SH, Kim SC, Song M, Lee J, Shin WS, Moon SJ, Bahng JH, Kotov NA, Jin SH (2011) Silver nanowire embedded in P3HT: PCBM for high-efficiency hybrid photovoltaic device applications. *ACS Nano* 5(4):3319–3325. <https://doi.org/10.1021/nn200469d>
- Kim M et al (2013) Development of the hybrid conjugated polymer solar cell based on GaN quantum dots. *Jpn J Appl Phys* 52:1–5
- Korona KP, Reszka A, Sobanska M, Perkowska PS, Wyszomolka A, Klosek K, Zytewicz ZR (2014) Dynamics of stacking faults luminescence in GaN/Si nanowires. *J Lumin* 155:293–297. <https://doi.org/10.1016/j.jlumin.2014.06.061>
- Kumar P, Guha S, Shahedipour-Sandvik F, Narayan KS (2013) Hybrid n-GaN and polymer interfaces: model systems for tunable photodiodes. *Org Electron Phys Mater Appl* 14: 2818–2825. <https://doi.org/10.1016/j.orgel.2013.08.003>
- Kwak ES, Lee W, Park N-G, Kim J, Lee H (2009) Compact inverse-opal electrode using non-aggregated TiO_2 nanoparticles for dye-sensitized solar cells. *Adv Funct Mater* 19(7): 1093–1099. <https://doi.org/10.1002/adfm.200801540>
- McDonald SA, Konstantatos G, Zhang SG, Cyr PW, Klem EJ, Levina I (2005) Solution-processed PbS quantum dot infrared photodetectors and photovoltaics. *Nat Mater* 4:138–142. <https://doi.org/10.1038/nmat1299>
- Noh J, Lee HY, Lim K, Ahn HS, Yi SN, Jeon H, Shin MJ, Yu YM, Ha DH (2017) Effects of P3HT concentration on the electrical properties of the Au/PEDOT:PSS/P3HT/n-GaN hybrid junction structure. *J Korean Phys Soc* 71:349–354. <https://doi.org/10.3938/jkps.71.349>
- Oh SH, Heo S-J, Yang J-S, Kim H-J (2013) Effects of ZnO nanoparticles on P3HT:PCBM organic solar cells with DMF-modulated PEDOT:PSS buffer layers. *ACS Appl Mater Interfaces* 5(22): 11530–11534. <https://doi.org/10.1021/am4046475>
- Park B-N, Uhlrich JJ, Kuech TF, Evans PG (2009) Electrical properties of GaN/poly 3-hexylthiophene interfaces. *J Appl Phys* 106:013713. <https://doi.org/10.1063/1.3159653>
- Pyrgotakis G. (2014) In *Properties of Group-IV, III-V and II-VI Semiconductors*, Springer Heidelberg, New York; B. Bhushan, Chapter 22, p. 784. <https://doi.org/10.1002/0470090340>
- Schroder D. K. (2009) In *semiconductor material and device characterization*, 3rd edn; Wiley: New York, Chapter 4, pp 185–187. <https://doi.org/10.1002/0471749095>
- Sobanska M, Fernández-Garrido S, Zytewicz ZR, Tchutchulashvili G, Gieraltowska S, Brandt O, Geelhaar L (2016) Self-assembled growth of GaN nanowires on amorphous Al_xO_y : from nucleation to the formation of dense nanowire ensembles. *Nanotechnology* 27:325601. <https://doi.org/10.1088/0957-4484/27/32/325601>
- Wang M, Li Y, Huang H, Peterson ED, Nie W, Zhou W, Zeng W, Huang W, Fang G, Su N (2011) Thickness dependence of the MoO_3 blocking layers on ZnO nanorod inverted organic photovoltaic devices. *Appl Phys Lett* 98:103305–103312. <https://doi.org/10.1063/1.3554381>
- Wierzbicka A, Zytewicz ZR, Kret S, Borysiuk J, Dłuzewski P, Sobanska M, Klosek K, Reszka A, Tchutchulashvili G, Cabaj A, Lusakowska E (2013) Influence of substrate nitridation temperature on epitaxial alignment of GaN nanowires to Si(111) substrate. *Nanotechnology* 24:035703. <https://doi.org/10.1088/0957-4484/24/3/035703>
- Yu G, Gao J, Hummelen JC, Wudl F, Heeger AJ (1995) Polymer photovoltaic cells—enhanced efficiencies via a network of internal donor–acceptor heterojunctions. *Science* 270(5243): 1789–1791. <https://doi.org/10.1126/science.270.5243.1789>
- Zhang Y, Liu H (2019) Nanowires for high-efficiency, low-cost solar photovoltaics. *Crystals* 9:87. <https://doi.org/10.3390/cryst9020087>

Publisher's note Springer Nature remains neutral with regard to jurisdictional claims in published maps and institutional affiliations.